Joint Contour Nets

Hamish Carr, *Member, IEEE,* and David Duke, *Member, IEEE,*

Abstract—Contour Trees and Reeb Graphs are firmly embedded in scientific visualization for analysing univariate (scalar) fields. We generalize this analysis to multivariate fields with a data structure called the *Joint Contour Net* that quantizes the variation of multiple variables simultaneously. We report the first algorithm for constructing the Joint Contour Net, and demonstrate some of the properties that make it practically useful for visualisation, including accelerating computation by exploiting a relationship with rasterisation in the range of the function.

Index Terms—Computational Topology, Contour analysis, Contour Tree, Reeb graph, Reeb space, Joint Contour Net, Multivariate.

1 Introduction

Simulations of physical phenomena have three major types of data: scalar, vector and multi-variate (multi-field). For scalar and vector data, many visualization techniques exist, from colour maps and glyphs to feature recognition and display. In recent years, these tools have included topological analysis to support visualization both analytically and algorithmically.

Research has only just begun to analyse the topological relationships of two or more properties. We report on the *Joint Contour Net*, an extension of the Reeb graph, that expresses the relationship between subsets of the domain with common properties. Developing this representation depends on early notions of the contour tree as the relationship between explicit contours or regions, however, rather than working directly from Morse Theory.

2 Scalar Field Topology

For a scalar function f on a continuous d-manifold M, a *level set* for isovalue $h \in I\!R$ is the inverse image of h:

$$f^{-1}(h) = \{x \in M : f(x) = h\} \tag{1}$$

In 2D, level sets are referred to as *isolines*, and in 3D, as *isosurfaces*. Since a level set may not be fully connected, we call a single connected component a *contour*. For a Morse function f, contours have one dimension less than the original manifold: e.g. contour lines on a topographic map have one dimension where the surface has two.

In practice, continuous Morse functions with infinite differentiability are intractable, and computational topology uses piecewise-continuous functions which may or may not be differentiable. These are usually defined on a mesh composed of polygonal, polyhedral or polytopal cells, where the value of f is only known at the vertices of the mesh. Morse behaviour is assured by simulation of simplicity [21], simulation of differentiability [20], and/or Discrete Morse Theory [22], which provides a combinatorial equivalent of Morse functions, reconstructing a smooth function for the purposes of analysis.

An alternate approach to constructing a smooth function is to work with a quantized representation (i.e. discretized in the range of the function). Weber et al. [45] relaxed the constraint of unique values, collecting isovalued regions and using them for topological analysis, an approach later extended to arbitrary dimension by Allili et al. [1]. More recently, Duffy et al. [14] have recognized that quantization of values in the range must also be taken into account: we will defer this to Section 5.

One form of analysis is the Reeb graph [34], which contracts contours to points, giving a graph description of connectivity. For simple domains, this is the contour tree [3]. Both structures are important in graphics and visualization because they capture the relationships of all contours of a function. Moreover, their combinatorial structure, based on equivalence classes between contours, subdivides the domain into regions of common behaviour, an important property for analysing data. They have been used for acceleration of isosurface algorithms [9], volume rendering [44], comparison of surface shapes [27] and of protein molecules [46], topological simplification of data sets [9], and reduction of high-dimensional data to landscape representations [43], [23].

Van Kreveld et al. [41] computed the contour tree for a mesh of N simplices in $O(N \log N)$ time in two dimensions, $O(N^2)$ in higher dimensions, by explicitly constructing a contour at high isovalues, then efficiently tracking changes as the isovalue varied. Carr et al. [8] reduced the simplicial mesh to a graph and computed connectivity of upper and lower level sets with isovalued sweeps and Tarjan's Union-Find algorithm [39], then merged the results into the contour tree. Chiang et al. [10] applied this to a graph constructed from monotone paths between critical points: a similar approach was used by Carr & Snoeyink [7] to extend to arbitrary mesh types. Pascucci & Cole-McLaughlin [32] and more recent work has generalised to parallel algorithms [32], [29], [28], while other work has described how to simplify the contour tree and reduce its size [9].

• *H. Carr and D. Duke are with the School of Computing, University of Leeds, Leeds, UK.*
E-mail: {h.carr,D.J.Duke}@leeds.ac.uk

For the Reeb graph, Pascucci et al. [33] gave a fast streaming algorithm editing the Reeb graph locally as simplices are added to a 2-manifold. While worst case runtime is at least $O(N^2)$, this is rare, and the algorithm is fast in practice. More recently, Tierney et al. [40] computed the Reeb graph in $O(N^2)$ by cutting a volumetric mesh along contours, applying the contour tree algorithm of Carr et al. [8], then repairing the cuts to construct the Reeb graph. Doraiswamy and Natarajan [12] have since extended this to arbitrary dimensions and reduced the memory overhead to $O(N)$, thus making the algorithm more efficient in practice. Most recently, $O(N \log N)$ time algorithms have also been described for both contour trees and Reeb graphs[24], [31], although earlier algorithms may still outperform them in practice.

3 Multi-Variate Topological Analysis

Although multi-variate computational topology is in its infancy, but four approaches can be identified: Jacobi sets, Reeb graph comparison, Reeb spaces, and range tessellation. For clarity, we will use *multi-field* to refer to functions of the form $\mathbb{R}^d \rightarrow \mathbb{R}^r$, and *multivariate data* to refer to computational discretizations of multi-fields, although this distinction is not common in the literature.

Jacobi sets were described by Edelsbrunner and Harer [17] as the systematic variation of critical points in multi-fields. These are extracted by taking a contour with respect to one variable, restricting another variable to that contour, and finding the critical points of the restricted function. As the first variable varies, the critical points sweep out paths in the domain. Moreover, Jacobi Sets can also be defined for time-varying data sets, and constructed in polynomial time [18]. Jacobi Sets can be simplified with rules similar to the contour tree [30].

A second approach uses the Reeb graph and contour tree to compare scalar fields. Hilaga et al. [27] used graph matching on Reeb graphs of different 2-manifolds to recognize shape similarities. Zhang et al. [46] extended this to 3-manifold functions, computing the contour tree with quantized data, then graph matching to recognize similar molecular shapes as expressed in the electrostatic potential field. Schneider et al. [37] took contour trees for two properties in a simulation, simplified the contour trees, then compared the overlap of features defined in the contour tree. While these papers have shown that the Reeb graph / contour tree can be used for comparison, they merely identify similarities between individual fields rather than giving overall structure.

A third approach starts by extending the Reeb graph to multivariate functions. Edelsbrunner et al. [19] did so, calling the result the *Reeb space*. We will illustrate an example of a Reeb space in Section 4, but observe that this is tightly linked with the mathematical analysis of singular fibers [35]. This analysis has been completed for functions of the form $\mathbb{R}^3 \rightarrow \mathbb{R}^2$ and $\mathbb{R}^4 \rightarrow \mathbb{R}^3$, but has not been accompanied by an algorithm for computation.

Edelsbrunner et al. [19] reported a complex and mathematically formalised algorithm for the Reeb space, lacking implementation details and asymptotic analysis. Moreover, the algorithm reported only works for 4 or fewer variables. In contrast, our approach works on principle for an arbitrary number of variables. More recently, Carlsson et al. [5] generalised a related notion, persistence, to higher dimensions. Their algorithm, however, is $O(m^2 n^4)$ where n is the number of properties and m is the number of cells in the input complex.

A fourth approach observed that statistics of isosurfaces were closely related to histograms [6]. Further developed by inverse gradient weighting [36], the latest work has shown that the relationship is defined by formal models of integration over interval volumes [14], typically defined by unit intervals in the range. This approach was used to improve scatterplot visualisations of continuous phenomena by using graphics hardware to project tetrahedra into the range of a function [2]. The relevance of this line of work is that it projects the graph of the function from an $m+n$-dimensional embedding space. As we will see later, this provides a method for accelerating computation of the Joint Contour Net.

In short, while some work has been done on multivariate topological analysis, what is lacking is a simple, efficient algorithm that computes usable structures. We report such an algorithm for the *Joint Contour Net* or *JCN*, which computes an approximate representation of multi-variate topology. Where $m > n$, the JCN is an approximation of the Reeb space. For $m = n$, the Reeb space is identical to the manifold of the function, but for $m < n$, the Reeb space is undefined. This is of particular concern when analysing scientific data, as it is common to compute many properties on a grid, so that $m << n$.

In contrast to the Reeb space, since the JCN is based on explicit subdivision of geometry, it can be computed even when $m \leq n$. For such cases, however, the JCN does not compute either the Reeb space or an approximation to it. Instead, it computes a graph representation of a remeshed version of the input data. We will, however, defer discussion of the details of this until Section 7, and start by generalising the notion of contour contraction.

4 Generalized Contour Contraction

It is straightforward to extend level sets to multi-variate functions. Instead of a scalar function $f : \mathbb{R}^m \rightarrow \mathbb{R}$, we shall consider scalar functions of the form $f : \mathbb{R}^m \rightarrow \mathbb{R}^n$, and define a level set for an isovalue $h \in \mathbb{R}^n$ to be:

$$f^{-1}(h) = \{x \in M \subseteq \mathbb{R}^m : f(x) = h\} \qquad (2)$$

As before, a contour is a connected component of a level set: one method of constructing the level set for a multi-variate isovalue $h = (h_1, \ldots, h_n)$ is to decompose f into scalar functions $f_1, \ldots, f_n$, and take the level set $f_1^{-1}(h_1)$ of the first component h_1 of the isovalue. As an example, we will define a bivariate function $f : A \subset \mathbb{R}^3 \rightarrow \mathbb{R}^2$ where $A = [-1,1] \times [-1,1] \times [0,1]$, and $f = (f_1, f_2)$, where $f_1(x,y,z) = \sqrt{x^2+y^2+z^2}$ is a spherical distance field centred at the origin, and $f_2(x,y,z) = z$ is

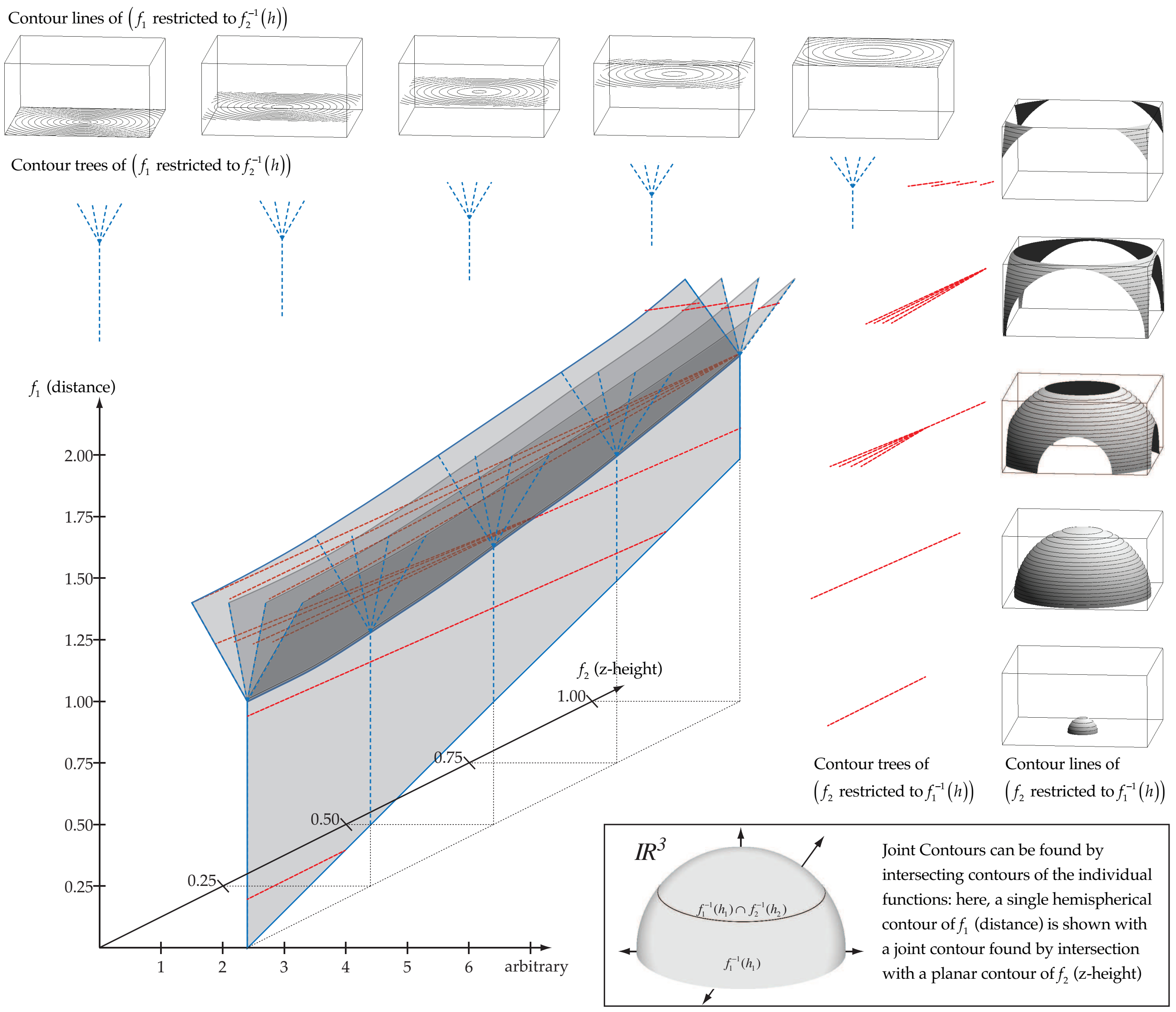
Contour lines of $\left(f_1 \text{ restricted to } f_2^{-1}(h)\right)$
Contour trees of $\left(f_1 \text{ restricted to } f_2^{-1}(h)\right)$
f_1 (distance)
2.00
1.75
1.50
1.25
1.00
0.75
0.50
0.25
f_2 (z-height)
1.00
0.75
0.50
0.25
1
2
3
4
5
6
arbitrary
Contour trees of $\left(f_2 \text{ restricted to } f_1^{-1}(h)\right)$
Contour lines of $\left(f_2 \text{ restricted to } f_1^{-1}(h)\right)$
IR^3
$f_1^{-1}(h_1) \cap f_2^{-1}(h_2)$
$f_1^{-1}(h_1)$

Joint Contours can be found by intersecting contours of the individual functions: here, a single hemispherical contour of f_1 (distance) is shown with a joint contour found by intersection with a planar contour of f_2 (z-height)

Fig. 1: The variation in level sets of a bivariate function can be expressed as a 2-manifold. Here, the function f_1 is a distance field, and the function f_2 is a height field. If we take an isosurface of f_1 then compute the Reeb graph of f_2 restricted to that surface, we get the sequence shown on the right. If we take an isosurface of f_2 then compute the Reeb graph of f_1 restricted to that surface, we get the sequence displayed along the top. Note that the Jacobi Set in this example is a subset of the edges of the Reeb Space projected back into the domain of f.

linear in z. As shown in Figure 1, the level sets of f_1 are hemispheres. We take as a second function $f_2(x, y, z) = z$, whose level sets are planes parallel to $z = 0$. Then, where the domain of the function is a 3-manifold, the level sets of f_1 and f_2 are 2-manifolds, possibly with boundary, and the level sets of f are 1-manifolds.

Figure 1 shows a small example of a bivariate function combining a distance function as f_1 and a height function as f_2. Isosurfaces of f_1 are hemispheres truncated to the domain A, (right). We show contours of f_2 on these isosurfaces, and their contour trees. As h_1 varies, the Reeb graph sweeps out the Reeb space, as shown. Equally, we can fix h_2 to get isosurfaces of f_2, in this case flat sheets. Plotting the contours of f_1 on these sheets, we get the sequence along the top. Here, the Reeb graph remains combinatorially consistent across all isovalues, but the values of the critical points change, and unsurprisingly, the Reeb space is again swept out.

As with the Reeb graph, any contour of f contracts to a point on the Reeb Space. And, since Jacobi Sets track the evolution of critical points of one property with respect to level sets of another, it then follows that the Jacobi Sets in this representation are a subset of the edges of the Reeb Space. To be precise, the critical points of f_1 or f_2 trace out the internal edges of the Reeb Space, but not necessarily all of the edges at the

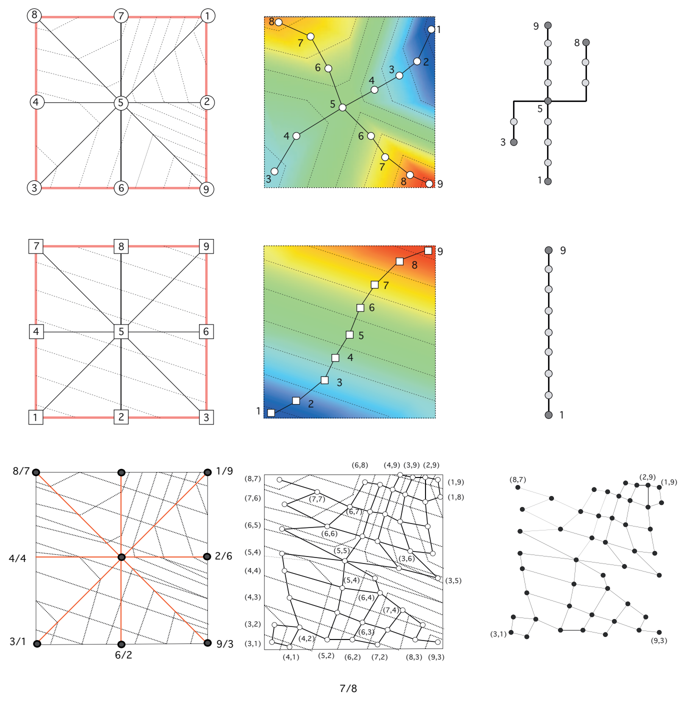

Fig. 2: Contour trees & JCN where $f : \mathbb{R}^2 \to \mathbb{R}^2$. Note how the JCN retessellates the manifold based on properties of the range rather than of the domain.

extreme values of the domain. In Figure 3, for example, computing the Jacobi set by analysing critical points of f_2 on isosurfaces of f_1 extracts all non-manifold edges of the Reeb space, but doing so by analysing critical points of f_1 on isosurfaces of f_2 does not extract the edges at minimum and maximum values of f_2. This occurs because the formal definition of Reeb space assumes a manifold without boundary, where our example has boundaries. Moreover, the Jacobi Set is usually shown in the domain of f, rather than in the Reeb Space.

This process of contracting contours to points has a drawback. Each time we fix an isovalue, we reduce the dimensionality of the graph of the function M by one. Thus, for $m \leq n$, our level sets will in general have dimension zero (points) or be empty, and the Reeb space will be the original manifold M.

5 Fragments and Slabs

Following Hilaga et al. [27], we use connected components of interval regions instead of contours. As observed by Duffy et al. [14], these are of full dimension, allowing intersection without dimension loss.

In Figure 2, we show a simple two-dimensional example. Here, instead of contour lines, we consider quantised contours: note how the dashed lines divide the mesh into regions of uniform connectivity. For clarity, we will use *fragment* to refer to such a region in a single cell, but *slab* to refer to such a region with respect to the entire mesh.

Since fragments are adjacent across cell boundaries, we collect them across cells to compute the contour tree, as shown on the sides of Figure 3. For quantized data on a simplicial mesh, the resulting tree is identical to the contour tree for a suitable choice of quantization.

For multi-variate data, we intersect slabs, as in Figure 3. We define a *Joint Level Set* at isovalue $h \in \mathbf{Z}^n$ as:

$$f^{-1}(h) = \{x \in M : round(f(x)) = h\} \quad (3)$$

For simplicial meshes, Joint Level Sets are not always connected, so we define a *slab* to be a single connected component of a Joint Level Set, in the same way that a contour is a single connected component of a level set.

In practice, we assume f is piecewise linear over a simplicial mesh. The slabs in each simplex are convex polytopes of full dimension - polygons in 2D, polyhedra in 3D. Combining the Joint Slabs of all simplices gives a slab decomposition of the entire domain, where adjacent slabs may or may not share the same discrete isovalue(s).

6 Joint Contour Nets

After extracting fragments for each simplex, each slab in the entire mesh is a union of connected fragments in different simplices. By computing fragment connectivity, we can therefore identify the slabs.

Since fragments are adjacent between cells, the *Joint Contour Graph G* is their dual graph. Here, nodes represent fragments and edges represent adjacencies. We then see that slabs are equivalent to connected components of isovalued nodes in the Joint Contour Graph.

We now perform a final reduction to find the connected components of each Joint Level Set, applying Tarjan's union-find [39] to edges of the Joint Contour Graph between isovalued nodes. This contracts components as identified by Reeb [34], and results in the *Joint Contour Net* or *JCN*, an abstraction which captures the systematic variation of all properties *simultaneously*.

Expressed in pseudo-code, the JCN algorithm consists of four phases: division of the domain into fragments, construction of the Joint Contour Graph G, union-find to find slabs (i.e. nodes in the JCN J), and a final phase to identify the edges of J. In practice, Phases I and II can be combined, as can Phases III and IV.

In Phase I, we start off with the mesh $M_0 = M$. At each iteration of Steps 4-8, mesh M_{i-1} has each cell divided with respect to property f_i, generating a new subdivided mesh M_i at each stage. When complete, M_n then holds the Joint Contour Slabs as defined above.

Phase II then constructs G from the fragment adjacencies. In practice, this will actually be computed during Phase I as part of the mesh data structure.

Phase III then applies Union-Find to identify the nodes of J. Initially, each representative in the Union-Find corresponds to a fragment - i.e. a node of G. As each fragment K_a is processed, each neighbour K_b is examined. If $f_i(K_a) = f_i(K_b)$ for all i, then the fragments have identical values, and an edge (a, b) is added to the Union-Find structure. When complete, the connected components of U represent the nodes of J.

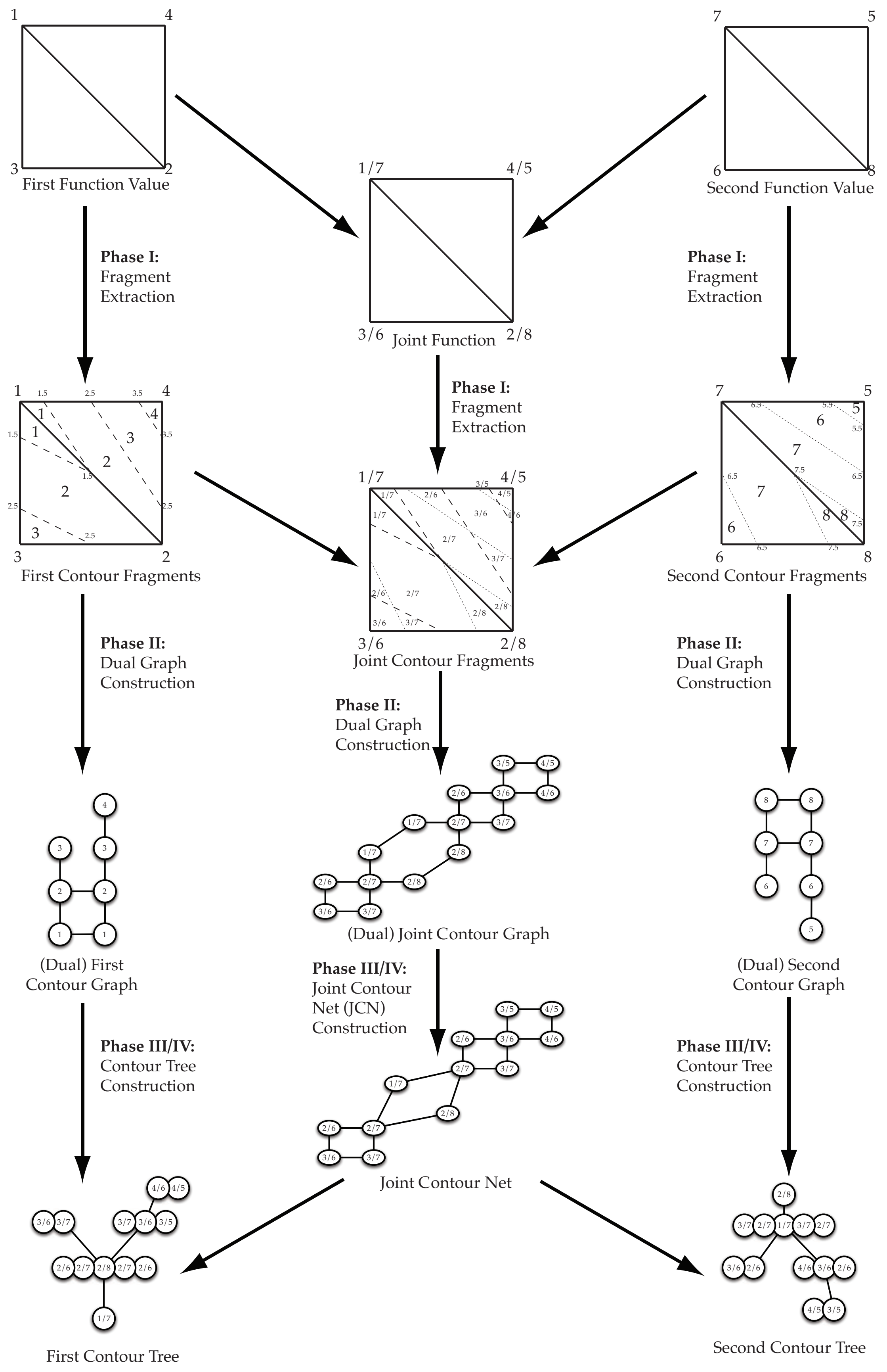

First Function Value
Second Function Value
Joint Function
Phase I: Fragment Extraction
First Contour Fragments
Joint Contour Fragments
Second Contour Fragments
Phase II: Dual Graph Construction
(Dual) First Contour Graph
(Dual) Joint Contour Graph
(Dual) Second Contour Graph
Phase III/IV: Contour Tree Construction
Phase III/IV: Joint Contour Net (JCN) Construction
Joint Contour Net
First Contour Tree
Second Contour Tree

Fig. 3: The Joint Function is divided into fragments by intersecting fragments for each individual function. The Joint Contour Graph G is then constructed as the dual graph of the fragments. Finally, the JCN J is constructed by contracting adjacent nodes in G with matching values. Note that the same contraction can be used to compute individual contour trees either from the JCN or directly from the individual Contour Graphs.

Algorithm 1 Algorithm for Computing JCN

```
Require: For simplicial mesh $M$ with functions $f_1, \ldots, f_n$ sampled to integer values at vertices of $M$, compute Joint Contour Net $J$
 1: PHASE I: CREATE FRAGMENTS
 2: Set $M_0 = M$
 3: for $i = 1$ to $n$ do
 4:     for all Cells $K \in M_{i-1}$ do
 5:         Initialize subdivided mesh $M_i \leftarrow \emptyset$
 6:         for $j = min(f_i|_K)$ to $max(f_i|_K)$ do
 7:             Add fragment $K \bigcap f^{-1}([j-0.5, j+0.5])$ to $M_i$
 8:         end for
 9:     end for
10: end for
Ensure: $M_n$ holds the fragments $F_i$ of $f$
11:
12: PHASE II: COMPUTE JOINT GRAPH $G$
13: for every fragment $F_i$ in $M_n$ do
14:     for every fragment $F_j$ adjacent to $F_i$ do
15:         Connect $F_1, F_2$ in $G$
16:     end for
17: end for
Ensure: $G$ is the dual graph of the fragments
18:
19: PHASE III: COMPUTE NODES OF JCN $J$
20: Let $N_f = Size(M_n)$ be the number of fragments in $M_n$
21: for $a = 1$ to $N_f$ do
22:     Initialize Union-Find: $U(a) = a$
23: end for
24: for $a = 1$ to $N_f$ do
25:     for all cells $K_b \in M_n$ adjacent to $K_a$ do
26:         if $f_i(K_a) = f_i(K_b) \forall 1 \leq i \leq n$ then
27:             Union($U, a, b$): Add $e = (a, b)$ to $U$
28:         end if
29:     end for
30: end for
Ensure: The representatives of $U$ are the slabs
31:
32: PHASE IV: COMPUTE EDGES OF JCN $J$
33: for $a = 1$ to $N_f$ do
34:     If $U(a) = a$, add $a$ as node to $J$
35: end for
36: for all edges $(K_b, K_a) \in G$ do
37:     if $f_i(K_a) \neq f_i(K_b)$ for any $1 \leq i \leq n$ then
38:         Add edge $(U(a), U(b))$ to $J$
39:     end if
40: end for
Ensure: $J$ now holds the Joint Contour Net
```

Finally, Phase IV strips out connected components of U to be used as nodes in J, then iterates through all cells K_a, K_b. For each pair of cells K_a, K_b that are which share a common $m-1$ dimensional face but do not share all isovalues, K_a cannot be in the same component of U as K_b, so an edge is added between their representatives in J (if already present, this operation has null effect). When complete, the JCN J has been constructed.

6.1 Algorithmic Analysis

To analyse this algorithm, we observe that it is dependent on the number N of simplices in the input mesh, the number Q_i of levels of quantization for each function f_i, the number r of functions defined, and the number d of input dimensions.

In Phase I, the loops over d and over the cells are functionally independent, so we assume each cell $K \in M$ is subdivided d times. The analysis then depends on the number of cells produced by intersecting $Q_1, \ldots, Q_d$ fragments. Barycentric interpolation of f on the simplicial mesh means that each set of fragments has parallel cuts: an easy upper bound on the number of fragments is $k = \prod_{i=1}^{d} Q_i$, although finer analysis might be found in the extensive literature on ham-sandwich cuts [16]. Accordingly, an upper bound on the computation time for Phase I is $O(rN_f)$ time where $N_f = O(kN)$. Here, the factor of r is because each cell is r-dimensional, so insertion of new cells is assumed to take $O(r)$ time.

Phase II iterates over every fragment in the mesh, then over every adjacent fragment. Assuming that retrieving each pair of adjacent fragments takes $O(1)$ time, as does storing them in the graph G, then this phase takes $O(N_e + N_f)$ time, where N_e is the number of edges in G, i.e. the number of adjacencies between fragments.

While graph connectivity means that N_e may be $O(N_f^2)$, a tighter bound exists. As we will see in Section 7, each fragment is the projection of a hypercube in the range onto the graph of the function - i.e. a form of rasterisation. Thus, each fragment is a convex distorted hypercube, possibly intersecting faces of the simplex.

Now, a hypercube of dimension r has $2r$ faces, and each side of the simplex can only add one face by truncation. Thus, each fragment can have at most $2r + d + 1$ faces, each of which contributes at most one edge to G. Thus, $N_e = O((2r + d)N_f)$, which is dimension-dependent but not quadratic in the number of fragments.

Phase III performs a Union-Find to identify slabs (nodes in the JCN J). Here, each adjacency is considered twice, but comparing n fields means that the cost will be $O(r)$ each time, for an overall cost of $O(rN_e)$. However, once the comparison is complete, at most N_e edges will be added to the union-find structure, giving an overall cost for this phase of $O(rN_e + N_e\alpha(N_e))$, where $\alpha(x)$ is the slow-growing inverse Ackermann function [39].

Phase IV iterates through the Union-Find U in at most $N_f\alpha(N_f)$ time to extract the vertices of J, then iterates through the adjacencies. Each comparison may take $O(r)$ time, giving at most $O(rN_e)$ time. Adding edges to J however is assumed to take $O(1)$ time, for an additional time of $O(N_e)$, which can be subsumed. Phase IV therefore takes $O(N_f\alpha(N_f) + rN_e)$ time in total.

Adding the costs, we get $O(N_f) + O(N_e + N_f) + O(rN_e + N_e\alpha(N_e)) + O(N_f\alpha(N_f) + rN_e)$. Since $N_e = O((2r+d)N_f)$, we can collapse this and get $O(rN_e + N_e\alpha(N_e))$.

While this is polynomial, the upper bound is very loose: the algorithm is primarily sensitive to k, the product of the number Q_i of quantization levels of the properties. Recent work [13] has shown that up to 95% of cells have only one quantization level, and most cells only have a few quantization levels. As a result, the worst-case behaviour is likely to occur only in a small number of cells, and can probably be bounded by examining the Jacobian of the function [14].

7 Properties

The JCN has a number of interesting properties that are likely to be useful for multi-variate analysis. Some of these properties are essentially theoretical and or algorithmic, while others are practical and related to known visualization tasks.

7.1 Theoretical Properties

It should be clear from the discussion in previous sections that the JCN and the Reeb Space are effective generalisations of the Reeb Graph and the Contour Tree and closely related to the analysis of singular fibers. Thus, the JCN can be viewed as part of the iterative process by which we explore the relationship between formal analysis, algorithmic development, and practical computations. Since the implications are broad, we list some of the issues we have identified, along with sketches of potential developments.

Reeb Graph / Contour Trees: Good generalisations can often be reflected back to the original example to develop further insights. Since the JCN generalizes Reeb Graph computations, new algorithms may be expected, although the work of Hilaga et al. [27] can now be recognized as essentially the same computation..

Pascucci showed a sort-based $\Omega(t\log(t))$ bound on contour tree computation [42]. However, quantization in the form of the radix sort escapes the general $O(t\log(t))$ bound on sorting. Since the JCN algorithm exploits quantization, so this lower bound does not apply.

A less obvious point is that most existing Contour Tree and Reeb graph algorithms rely on a global sort order of the vertices, and that this global property hampers parallel computation. Our algorithm processes each simplex independently in Stage I: as a form of rasterisation, fragment creation can be parallelized. While further work is needed to produce an efficient implementation, the absence of any global ordering means that the new algorithm can be expected to parallelize relatively easily. The mapping from discrete fragments onto JCN nodes should replace the global sorting step of existing algorithms with a radix sort, which is easy to parallelize.

Re-meshing: As identified by an anonymous reviewer, the effect of the fragment and slab computation is to retessellate the function with respect to range properties instead of domain properties. To see this, consider the bottom row of Figure 2, in which the left hand image shows the original mesh with each cell broken up into fragments, and the middle image shows the slabs. Since these slabs fill the space, they constitute a remeshing of the domain. Moreover, one can project them onto the graph $Gr(f)$ of the function and observe that each slab constitutes an identifiable fragment of $Gr(f)$.

However, since this small example is $\mathbb{R}^2 \rightarrow \mathbb{R}^2$, $Gr(f)$ is embedded in $\mathbb{R}^4$, which is difficult to illustrate. We instead show a simplified example in Figure 4 of a function $g : \mathbb{R} \rightarrow \mathbb{R}^2$: i.e. a space curve in $\mathbb{R}^3$, in this instance a helix, i.e. $g(x) = (y = cosx, z = sinx)$. Since our fragments and slabs are defined by taking intervals in the ranges of y, z, the effect of this is to retessellate the graph into the coloured segments shown (note that they have no thickness except for the purposes of illustration).

Given this retessellation, we can now see that as the number of slabs increases, the tessellation will converge to the original space, with each coloured region in general representing a slab composed of one or more fragments. And, since the JCN is the dual edge graph of these slabs, convergence to the connectivity of the Reeb Space then follows, although true convergence requires handling higher-order faces as well.

Relationship to Reeb Space: In Section 4, we observed that $m > n$, $m = n$ and $m < n$ need to be treated separately. For $m > n$, the Reeb Space, the JCN and the singular fiber analysis are well defined, and the JCN is an approximation of the connectivity of the Reeb space.

For $m = n$, joint contours or fibers (i.e. inverse images of values in the range) will in general be of dimension 0 - i.e. finite collections of individual points, and the Reeb space is identical to the graph of the function. For the same reason, singular fiber analysis does not handle this case at present. The JCN, however, can still be computed, as it is explicitly based on geometric subdivision.

For $m < n$, no Reeb space is defined, but the JCN can still be computed, as shown in Figure 4. Since the JCN remeshes $Gr(f)$, and varying mesh representations is of practical value, we expect that geometric [9] information can be captured and analysed this way.

For example, in the JCN, the density (resolution) of the tessellation will be related to the rapidity with which the quantization changes - i.e. to the Jacobian of f. We note that high gradients in volumetric data lead to aliasing problems, and observe that, in previous work, aliasing was resolved by exploiting continuity [14]. As a result, we may be able to look at local correlation of variables by examining the density in the domain of the slabs. Second, there may be graph algorithms which use properties of the JCN to identify boundaries that do not map to isovalued boundaries or Joint Contours. And third, the slab density and the related graph representation may still be useful even for cases where $m < n$, and the Reeb Space is equivalent to the original domain.

7.2 Practical Properties

In addition to theoretical relationships, another set of properties can be identified, all related either to practical

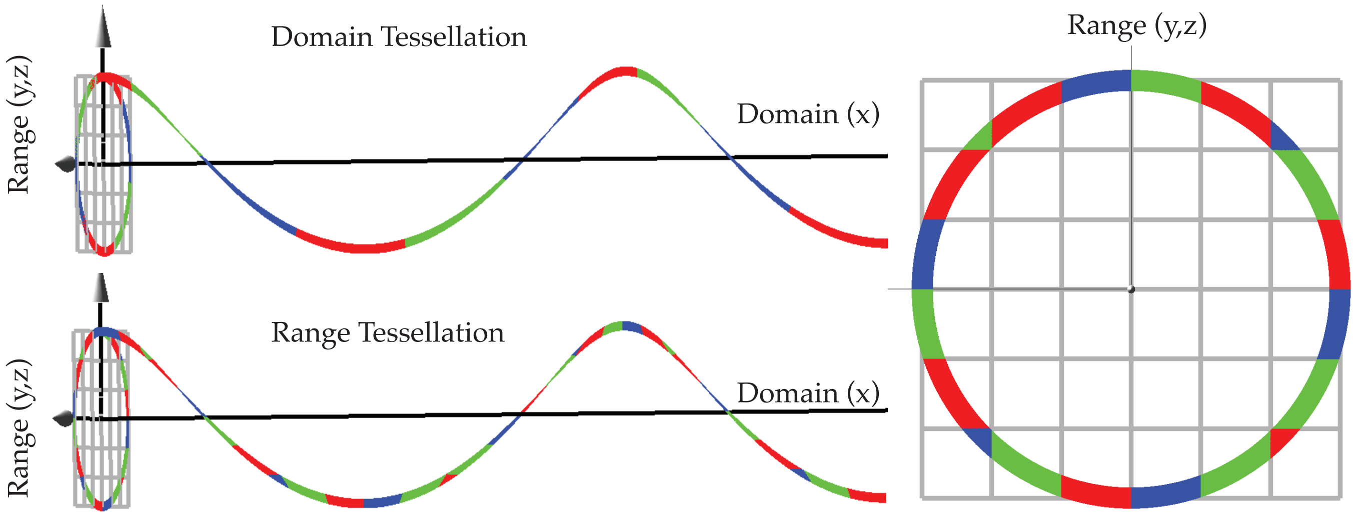

Fig. 4: A function $g : I\!R \rightarrow I\!R^2$ that defines a helix. At left, $Gr(g)$ is shown as a space curve, once with segments coloured by uniform tessellation of the domain (top), once coloured by uniform tessellation of the range (below). At right, $Gr(g)$ shown by projection into the range: the same coloured segments now become fragments with respect to the range, even though multiple components may project to the same range cell. As a result, computation of the JCN is equivalent to rasterising $Gr(g)$ with respect to pixels in the range (as with Continuous Scatterplots [2]. Note that the segments are of zero thickness, but are exaggerated for the purposes of illustration.

properties of the Reeb Graph / Contour Tree, or to potential visualization tasks:

Representation of Multi-Variate Contours: Each univariate or multi-variate contour corresponds to a connected set in the JCN. This follows directly from the characterization of the slabs as equivalence classes of contours used in the proof above.

Extraction of Contours: Either uni-variate or multivariate slabs can be extracted using the JCN. Again, from the characterization of the slabs as equivalence classes of contours, this follows provided that we store a single fragment as a representative of each slab (i.e. node in the JCN). Extracting a contour can then be done with depth-first or breadth-first search through the cells of the mesh, following to adjacent fragments. Alternately, since the fragment adjacency is encoded in the Joint Contour Graph, a simple flood-fill can be used to extract all relevant fragments.

Contours and Features: Uni-variate contours cut the domain into pieces, thus defining features: moreover, the nesting relationship induced by this property is one of the definitions of the Contour Tree [3]. Most multivariate contours, however, do not cut the domain into pieces. However, and perhaps more interestingly, not all algorithms use contours. Instead, methods such as level sets use alternate formulations to construct boundary surfaces that separate an inside from an outside, or otherwise segment the domain into features.

Given any such boundary that cuts the domain into pieces, let B be the set of slabs through which the boundary passes. Since B is a superset of the boundary, removing it will also disconnect the domain. Since each slab corresponds to a JCN node, removing the nodes corresponding to B must also disconnect the JCN.

Inversely, since each node in the JCN represents a slab in space, and the edges of the JCN represent face-adjacencies of the slabs, a connected set N of nodes in the JCN represents a contiguous region of the domain. And, if N is a cut set for the JCN, each cut component will correspond to a disjoint region of the domain - hence, cut sets in the JCN induce cuts in the domain that separate potential features. It then follows that graph properties such as minimal cut sets in the JCN are likely to reveal interesting boundary phenomena in the multifield f.

Representation of Sub-Nets: For any subset of the variables f_i, the JCN for those variables can be computed by repeating Phases III & IV, using the JCN for all variables as the input graph, and collapsing nodes that match on the chosen subset of variables. Thus, partial relationships between variables can be found directly from the JCN. In particular, the Reeb Graph and Contour Tree for any variable can be extracted directly from J.

Quantization Simplifies: Varying the level of quantization simplifies the Joint Contour Graph. This is a direct consequence of the construction being a form of retessellation of the graph of the function. Simplified versions of the JCN then follow, as they are constructed from a simplified Joint Contour Graph in the first place.

Moreover, if coarse quantization levels use a subset of the boundaries at the finest level, adaptive refinement can be used to compute the Joint Contour Graph. In short, the quantization need not be uniform in the range, and it should even be possible to vary it according to topological properties of a coarsely computed version.

Also, topological simplification can be driven by suit-

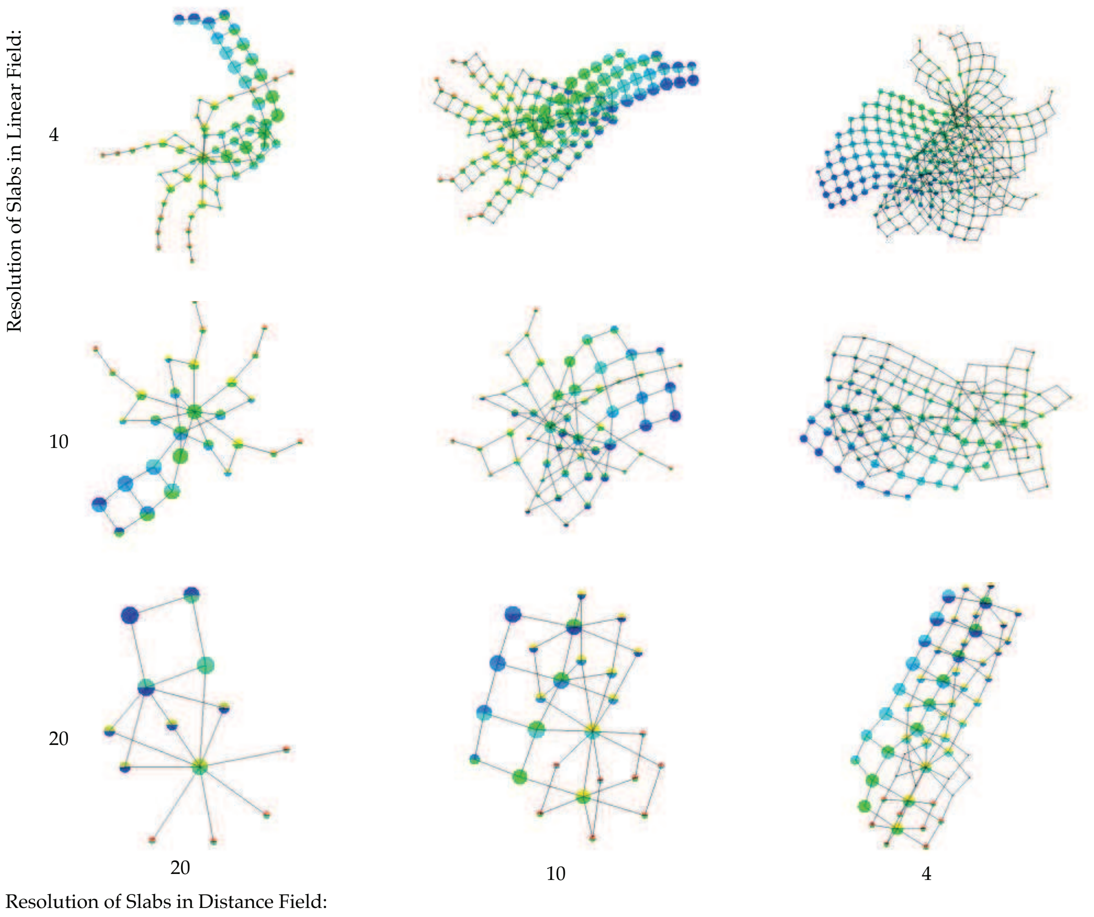
Resolution of Slabs in Linear Field:
4
10
20
20
10
4
Resolution of Slabs in Distance Field:

Fig. 5: Effects of Quantization. The bivariate function $f : \mathbb{R}^3 \rightarrow \mathbb{R}^2$ shown in Figure 1 was sampled onto a tetrahedral mesh, and the JCN was computed with slab intervals of 20, 10 and 4 with respect to both properties. Note that as the slab interval decreases, the JCN converges to the manifold structure of Figure 1, as predicted. Graph layout is still an issue, as appropriate aesthetics are as yet unclear. Here and elsewhere unless otherwise stated, force-directed layout has been used (vtkForceDirectedLayoutFilter). Each layout uses the same random seed for initial positioning of vertices, but final results are sensitive to graph structure and there is no guarantee of layout consistency between structurally similar graphs.

able geometric measures [9], topological simplification can be driven by geometric information, as with the Contour Tree and much of the existing literature on remeshing. We also note that this idea – of varying the level of simplification, was prefigured by Hilaga et al. [27] and Zhang et al. [46] in their computations of coarser versions of the Reeb Graph and Contour Tree.

We show the effects of varying levels of quantization in Figure 5 using a synthetic two-field dataset. One field has constant values along each row, decreasing from top to bottom. The second field approximates a radial distance function, with the origin at the center of the mesh. As expected, the combined fields exhibits a four-fold symmetry; the figure shows that the JCN captures this feature even at quite coarse resolutions.

This ability of the JCN to discriminate features at coarse levels has already been exploited to analyse data arising in a specific domain problem, identifying the point of "scission" within simulations of heavy nuclei [15], derived from density functional theory (DFT). Figure 6 uses four JCNs to show the joint topological structure of proton and neutron density fields for fermium. These JCNs were computed from volumetric density data in turn derived from two sites along a trajectory in the high-dimensional space underlying DFT. The data are 8-bit samples; the top row was constructed using a slab width of 32, the lower row a slab width of 16. Rectangles highlight the position of a significant combinatorial event, the point at which a nucleus split into multiple (in this case two) fragments.

Graph Layout: We have deliberately not considered the design and implementation of graph layout specific to the JCN. Any such layout algorithm needs to begin with an understanding of the graph aesthetics, that is, the mapping between layout and relevant information encoded within the JCN, and how these might interact with more generic criteria from graph perception and comprehension. Having identified the JCN as an ab-

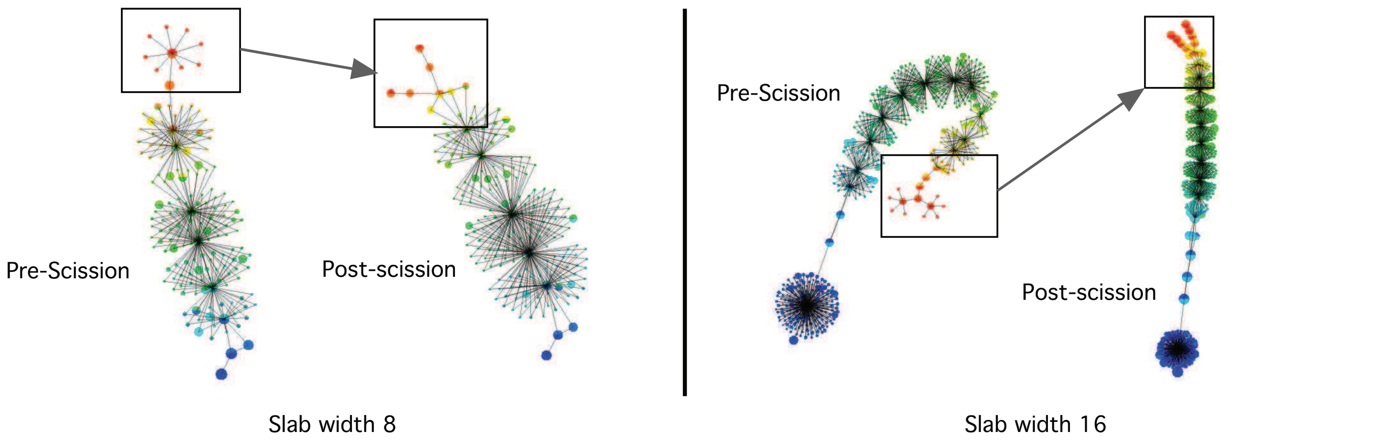

Fig. 6: Joint Contour Nets of nuclear density data used to locate the scission (nucleus fragmentation) point along a trajectory in a higher-dimensional space defined by density functional theory. JCN's in the left column are pre-scission, those in the right are post-scission. Identification of combinatorial change in the JCN structure is marked by boxes. The top row is computed at slab width 16, the second row at slab width 8. Although the bottom-left figure shows some branching in the structure, the scission point is marked by the appearance of extended linear branches, a hypothesis supported by blind calibration experiments carried out by our physics collaborators [15].

straction for multifield topology, further work will be needed to map out structural properties of the network that should be highlighted in its external representation. There is clearly a "chicken and egg" problem here; we break the cycle by using force-directed layout in the first instance, on the grounds that there has been success in using the algorithms to highlight structural symmetry and other regularities in both local and global network structure. As recent work on layout of Contour Trees demonstrates [25], it can take signficant time and effort between identifying important abstractions, and having effective algorithms for their representation.

Summary: In short, many properties of the Contour Tree that have been applied for visualization have direct equivalents in the JCN, and we can predict that this will allow the development of topological tools for multifield visualization. As an example of the use of the JCN to analyse multivariate data, Figure 6 shows illustrations from an application paper [15] applying JCN analysis for nuclear fission simulations. Figure 7 shows the JCN for a vector field from the meso-scale atmospheric simulation [26]: the relationship between the JCN (operating on arbitrary collections of scalar fields), and tools for the topological analysis of 'multifields' representing vector and tensor quantities, is an interesting but open question.

8 Implementation: Base Algorithm

The JCN algorithm has been implemented as a filter for the Visualization Toolkit (VTK) [38]. As proof-of-concept, our initial implementation favours brute-force simplicity and generality over performance. The filter takes as input an unstructured grid, which is assumed to contain simplicial cells (either all triangles, or all tetrahedra), and generates three outputs:

1) the Joint Contour Net, as an undirected graph
2) (optionally) each individual fragment, as a polygonal mesh
3) (optionally) each contour slab, as a polygonal mesh

Dataset processing goes through three phases. In the first, simplicial cells are converted into fragments. Internally we maintain a queue of (partially fragmented) polytopes (polygons or polyhedra, depending on dimensionality). We iterate over cells, initialising the fragment queue to the cell itself. Then for each scalar field and threshold, we run through the fragment queue, cutting each polytope against the current field threshold, and requeuing the resulting fragments. Once a polytope cannot be clipped further, it is placed in the output. Second, the dual graph of fragments is computed using tables from the first phase that record information about shared fragment edges/faces. The dual graph is then simplified by collapsing adjacent nodes with the same combination of field values. Last, Joint Contour Slab boundaries are computed by iterating over fragment facets (edges or faces) and discarding those internal to a slab.

Testing has been carried out on both synthetic datasets (allowing for verification of the JCN implementation), and on the real fermium and plutonium datasets referred to in the application paper [15]. In the case of single-field data (e.g. the nucleon dataset), the JCN analysis shows that the JCN reduces to a tree, as expected. As a baseline for future work, Tables 1 and 2 set out the results of runtime tests. The former reports dataset sizes, while the latter gives performance measurements: the width (granularity) of each slab across each data dimension; the total number of fragments generated; the number of slabs; and the size of the resulting contour net.

Table 2 shows that the relationship between dataset size, slab granularity and performance indicators is not straightforward. Doubling the granularity does not automatically double the runtime, but depends on the

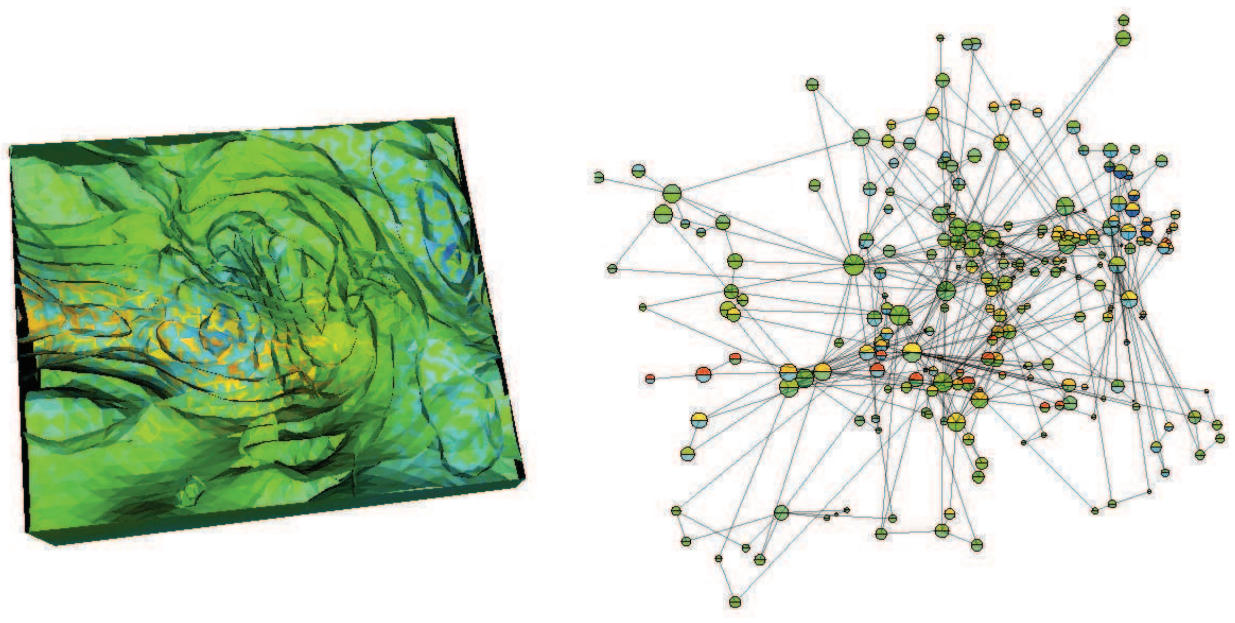

Fig. 7: Fields U and V (horizontal vector components) from time Step 11 of the Limited Area Meso-Scale Prediction System (LAMPS) data set [26]. In this example JCN nodes on the right are positioned in a 3D space at the barycenter of the corresponding slabs on the left. The circular structure in the JCN appears to correspond to rotational movement in the simulation: we expect to explore this further in future work.

TABLE 1: Dataset Statistics

Dataset	Spatial Dimensions	Simplices	Field Widths
simple	3×3	8	9×9
sphereBox	$11 \times 6 \times 11$	2,500	$[0,6] \times [-4,71]$
nucleon	$41 \times 41 \times 41$	320,000	256
fermium	$19 \times 19 \times 19$	29,160	$256 \times 256 \times 256$

underlying field. For fermium, the trials reported involve doubling the resolution of three fields, so in the worst case we might expect an 8-fold increase in runtime and output size. Other than in the transition to (1,1,1), runtime growth is closer to a factor of 2, while changes in JCN node and edge size vary by around 5. These figures should be treated with caution, since our implementation was proof-of-concept rather than production-oriented. For example, it explicitly constructs and discards large volumes of fragment geometry.

9 Raster Acceleration

As noted above, the effect of the JCN is to tessellate the function manifold with respect to the range of the function rather than the domain. Moreover, since the slabs are defined by intervals in each univariate channel in the range, the effect is to project a regular grid in the range onto the function manifold, with each Joint Contour Slab corresponding to a Euclidean box in the range. For a function $f : \mathbb{R}^2 \to \mathbb{R}^2$, these boxes are pixels, and the relationship to Bachthaler & Weiskopf's work on continuous scatterplots [2] becomes apparent.

Since the neighbourhood relationships of pixels are easily described, this simplifies the computation of the JCN by transforming it to a well understood rasterisation problem. For two dimensions, this immediately gives an effective method of computing the JCN without explicitly extracting geometric slabs. This gives a full order of magnitude speed up compared with the naïve algorithm, at a slight cost in accuracy because rasterisation algorithms do not necessarily rasterise every pixel *intersected* by the primitive. However, since the JCN is already an approximate computation, this is an acceptable cost in some circumstances, and does give the basis for further acceleration once efficient and accurate rasterisation algorithms are available in arbitrary dimensions.

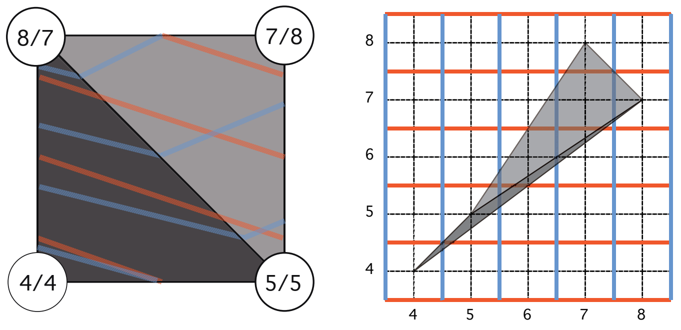

Fig. 8: Rasterising the JCN. Each slab (left) corresponds to a Euclidean box (pixel) in the range (right), transforming this into a rasterisation problem. Each pixel rasterised corresponds to a fragment.

Figure 9 shows that rasterization preserves important topological features. These figures, based on the application in physics illustrated in Figure 6 [15], show the

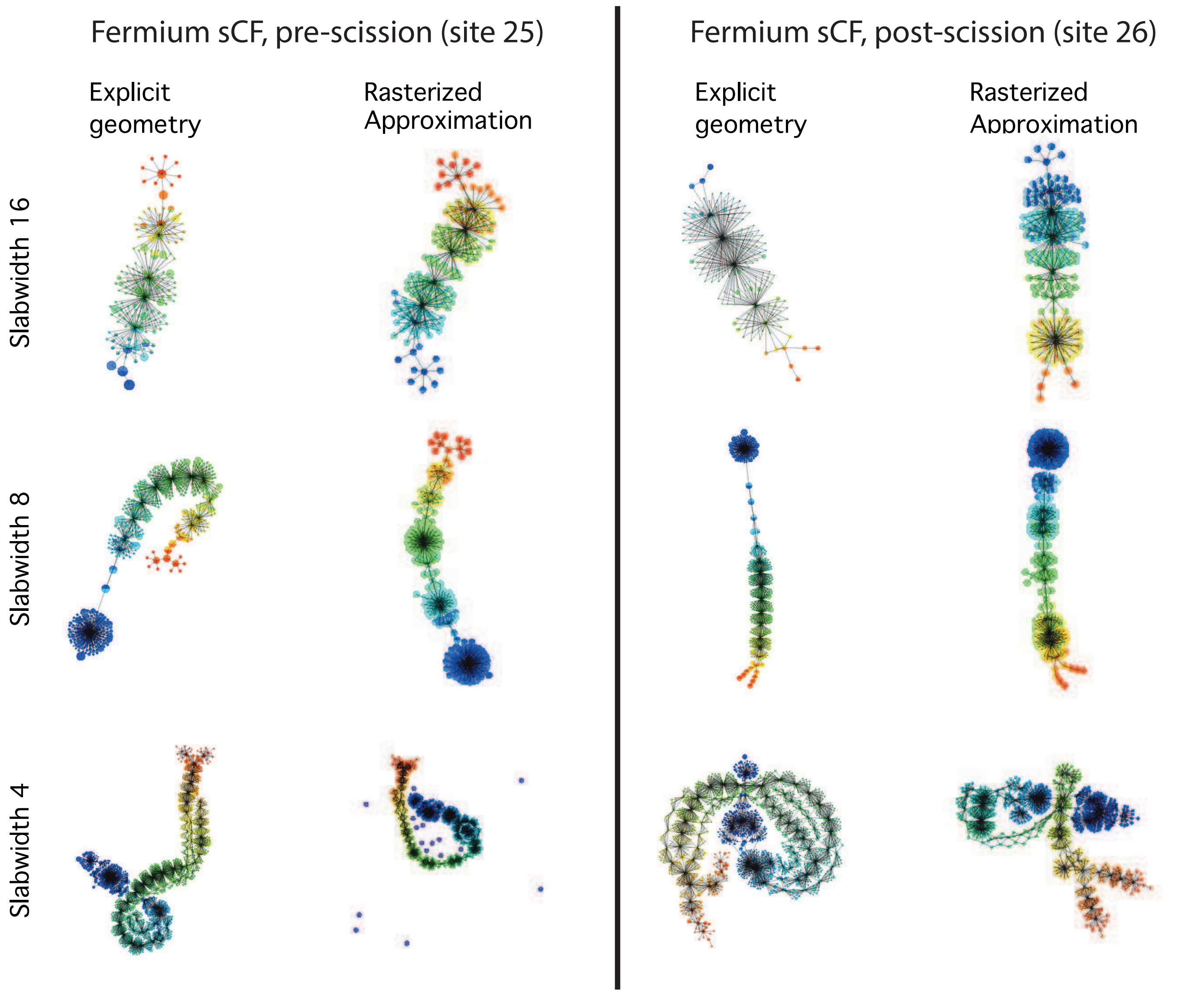

Fig. 9: Comparison between explicit geometric construction of JCN, and rasterization for two different methods of inter-cell linking, both before (site 25) and after scission (site 26) in fermium sCF dataset [15]. Differences in the graph structure, particularly at slabwidth 4, are a result of the approximation in rasterization (visible by comparing graphs at high slabwidth), and compounded by sensitivity of force directed layout to graph structure.

scission point of a fermium nucleus, at which a single nucleus breaks into two fragments. Within each figure the top row shows the images generated using explicit geometric construction of JCN slabs, for three different levels of quantization (slab widths 16, 8, and 4). The bottom row shows the rasterised approximation, with major features clearly carrying over, but some artifacts in the form of isolated nodes. We have not included a qualitative comparison of the LAMPS data, as for this JCN the appropriate layout positions nodes at the barycenter of the corresponding geometric slab [15], and the raster implementation does not generate this data.

Dataset statistics and timing information are shown in Table 3, using the system configuration described in Table 2. For the nucleon data (which consists of a single scalar field), we note that the geometric and raster implementations return the same (tree) structure, and that the performance gain from the raster implementation improves substantially as finer levels of quantization.

10 Conclusions and Future Work

We have shown that the contour tree can be extended to multi-variate fields, opening up possibilities for topological analysis and visualization. In the future, we will refine algorithms for computing the JCN, methods of simplification and secondary analysis of the JCN, and methods for visualizing the underlying multi-variate data. We expect that many of the techniques that work for the contour tree and Reeb graph will then extend to the JCN. It has also become clear that while the JCN itself captures topological and geometric structures of

TABLE 3: Runtime statistics for rasterization, for a subset of the 2D range datasets from 2. Statistics for explicit geometry have been copied over for ease of comparison. Rasterization results for lower-dimensional (1D) datasets are also shown. Speedup was computed by taking the ratio of the times stated.

		Explicit Geometry				Rasterization				
Dataset	Quantization	nr-frags	nr-nodes	nr-edges	time	nr-frags	nr-nodes	nr-edges	time	Speedup
Fermium sc25	16,16	83,744	163	307	2.75	104,619	157	280	0.59	4.7
Fermium sc25	8,8	144,576	547	1,063	5.32	142,451	268	497	1.01	5.3
Fermium sc25	4,4	264,320	1,749	3,501	11.44	266,817	917	1,769	2.16	5.3
Fermium sc25	2,2	531,552	8,810	18,189	28.43	547,360	2,755	5,536	6.61	4.3
Fermium sc25	1,1	1,103,632	38,351	85,064	79.00	1,193,128	9,042	18,216	24.72	3.2
LAMPS 9 (U,V)	10, 10	197,197	241	490	5.96	163,428	310	444	1.54	3.8
Nucleon	32	405,556	48	47	8.35	402,104	48	47	1.62	5.2
Nucleon	16	505,932	64	63	11.33	500,831	64	63	1.72	6.6
Nucleon	8	703,557	103	102	17.61	774,496	103	102	1.94	9.1
Nucleon	4	1,095,526	166	165	29.80	1,091,981	166	165	2.44	12.2

TABLE 2: Runtime Statistics. All timings were performed on a 2GHz MacBook Air with 8GB memory, running OSX 10.7.5, and using VTK 5.10 configured as a release build: times are substantially lower than previously reported[15], which used a debug build. Fermium timings in this table use site 25 of the sCF trajectory, and proton and neutron density fields (see [15] for details). To broaden the results, a further set of timings has been included from a different trajectory from the same dataset, site aEF. This uses a third, derived, field (total density) that was not required for the study reported in [15]. LAMPS timings are for time step 9 of the dataset.

dataset	Slab widths	Runtime	Fragments	Slabs	Edges
simple	(1,1)	0.20s	73	46	71
simple	(0.2,0.2)	0.23s	945	810	1,515
sphereBox	(4,4)	0.48s	9,068	68	97
sphereBox	(2,2)	0.70s	15,900	199	318
sphereBox	(2,1)	0.71s	15,900	329	576
sphereBox	(1,2)	1.00s	27,300	400	647
sphereBox	(1,1)	1.10s	27,300	650	1,145
nucleon	32	8.42s	405,556	48	47
nucleon	16	11.80s	505,932	64	63
nucleon	8	17.84s	703,557	103	102
fermium sc25	(32,32)	1.60s	53,448	16	15
fermium sc25	(16,16)	2.66s	83,744	103	307
fermium sc25	(8,8)	5.32s	144,576	547	1,063
fermium sc25	(4,4)	11.44s	264,320	1,749	3,501
fermium sc25	(2,2)	28.43s	531,552	8,810	18,189
fermium sc25	(1,1)	79.00s	1,103,632	38,351	85,064
fermium ae10	(32,32,32)	1.94s	59,928	14	13
fermium ae10	(16,16,16)	3.66s	97,728	195	373
fermium ae10	(8,8,8)	7.60s	172,424	852	1,808
fermium ae10	(4,4,4)	18.48s	325,296	5,934	13,596
fermium ae10	(2,2,2)	25.86s	681,240	31,711	81,341
fermium ae10	(1,1,1)	183,80s	1,494,731	194,109	599,581
LAMPS 9 U,V	(10,10)	5.96s	197,197	241	409
LAMPS 9 U,V	(20,20)	3.75s	142,891	82	117
LAMPS 9 P,T,H	(10,100,4)	25.6s	237,168	387	823
LAMPS 9 P,T,H	(20,200,8)	15.9s	158,501	83	145

the graph of the function, extracting and storing a fully meshed complex [4] will be useful for some problems, but that for other problems, such as parameter space analysis, construction from graph structures such as the Gabriel graph [11] will be more fruitful.

We also intend to study the relationship between the JCN and Jacobi Sets, and consider whether there is an equivalent to the Morse-Smale Complex. While the current work has used existing two-dimensional rasterisation methods, future work will necessarily extend to higher-dimensional rasterisation, which will be applicable not only to the JCN, but also to many other multi-variate analysis and visualisation techniques.

Acknowledgements

Acknowledgements are due to Bob Laramee and Eugene Zhang, presentation of whose work triggered this line of thought. Our initial results on the nuclear fission datasets were produced in collaboration with Aaron Knoll, Nicolas Schunck, Hai Ah Nam, and Andrzej Staszczak. This work is supported by the UK Engineering and Physical Sciences Research Council under Grant EP/J013072/1. Thanks are also due to the anonymous reviewers for suggestions on how to improve the presentation and for the significant observation that the JCN re-tessellates the graph of the function with respect to the range.

References

[1] M. Allili, M. Ethier, and T. Kaczynski. Critical Region Analysis of Scalar Fields in Arbitrary Dimensions. In *Proceedings of Visualization and Data Analysis 2010*, pages 753008–12, 2010.

[2] S. Bachthaler and D. Weiskopf. Continuous Scatterplots. *IEEE Transactions on Visualization and Computer Graphics*, 14(6):1428–1435, 2008.

[3] R. L. Boyell and H. Ruston. Hybrid Techniques for Real-time Radar Simulation. In *Proceedings, 1963 Fall Joint Computer Conference*, pages 445–458. IEEE, 1963.

[4] D. Canino, L. de Floriani, and K. Weiss. IA*: An Adjacency-Based Representation for Non-Manifold Simplices in Arbitrary Dimensions. *Computers and Graphics*, 35(3):747–753, 2011.

[5] G. Carlsson, G. Singh, and A. Zomorodian. Computing Multidimensional Persistence. *Journal of Comp. Geometry*, 1(1):72–100, 2010.

[6] H. Carr, B. Duffy, and B. Denby. On Histograms and Isosurface Statistics. *IEEE Transactions on Visualization and Computer Graphics*, 12(5):1259–1266, September/October 2006.

[7] H. Carr and J. Snoeyink. Representing Interpolant Topology for Contour Tree Computation. In H.-C. Hege, K. Polthier, and G. Scheuermann, editors, *Topology-Based Methods in Visualization II*, Mathematics and Visualization, pages 59–74. Springer, 2009.

[8] H. Carr, J. Snoeyink, and U. Axen. Computing Contour Trees in All Dimensions. *Computational Geometry: Theory and Applications*, 24(2):75–94, 2003.

[9] H. Carr, J. Snoeyink, and M. van de Panne. Flexible Isosurfaces: Simplifying and Displaying Scalar Topology Using the Contour Tree. *Computational Geometry: Theory and Applications*, 43(1):42–58, 2010.

[10] Y.-J. Chiang, T. Lenz, X. Lu, and G. Rote. Simple and Optimal Output-Sensitive Construction of Contour Trees Using Monotone Paths. *Computational Geometry: Theory and Applications*, 30:165–195, 2005.

[11] C. D. Correa and P. Lindstrom. Towards Robust Topology of Sparsely Sampled Data. *IEEE Transactions on Visualization and Computer Graphics*, 17(12):1852–1861, 2011.

[12] H. Doraiswamy and V. Natarajan. Computing Reeb Graphs as a Union of Contour Trees. *IEEE Transactions on Visualization and Computer Graphics*, page DOI: 10.1109/TVCG.2012.115, 2012.

[13] B. Duffy and H. Carr. Interval based data structure optimisation. In *Proceedings, Theory and Practice of Computer Graphics 2010*, pages 151–158, 2010.

[14] B. Duffy, H. Carr, and T. Möller. Integrating Histograms and Isosurface Statistics. *IEEE Transactions on Visualization and Computer Graphics*, 19(2):263–77, 2013. DOI: 10.1109/TVCG.2012.118.

[15] D. Duke, H. Carr, A. Knoll, N. Schunck, H. A. Nam, and A. Staszczak. Visualizing nuclear scission through a multifield extension of topological analysis. *IEEE Transactions on Visualization and Computer Graphics*, 18(12):2033–40, 2012.

[16] H. Edelsbrunner. *Algorithms in Combinatorial Geometry*. Springer-Verlag, 1987.

[17] H. Edelsbrunner and J. Harer. Jacobi Sets of Multiple Morse Functions. In *Foundations in Computational Mathematics*, pages 37–57, Cambridge, U.K., 2002. Cambridge University Press.

[18] H. Edelsbrunner, J. Harer, A. Mascarenhas, V. Pascucci, and J. Snoeyink. Time-Varying Reeb Graphs for Continuous Space-Time Data. *Computational Geometry*, 41(3):149–166, 2008.

[19] H. Edelsbrunner, J. Harer, and A. K. Patel. Reeb Spaces of Piecewise Linear Mappings. In *Proceedings of ACM Symposium on Computational Geometry*, pages 242–250., 2008.

[20] H. Edelsbrunner, J. Harer, and A. Zomorodian. Hierarchical Morse Complexes for Piecewise Linear 2-Manifolds. In *Proceedings, 17th ACM Symposium on Computational Geometry*, pages 70–79. ACM, 2001.

[21] H. Edelsbrunner and E. P. Mücke. Simulation of Simplicity: A Technique to Cope with Degenerate Cases in Geometric Algorithms. *ACM Transactions on Graphics*, 9(1):66–104, 1990.

[22] R. Forman. Discrete Morse Theory for Cell Complexes. *Advances in Mathematics*, 134:90–145, 1998.

[23] W. Harvey and Y. Wang. Generating and Exploring a Collection of Topological Landscapes for Visualization of Scalar-Valued Functions. *Computer Graphics Forum*, 29(3), 2010.

[24] W. Harvey, Y. Wang, and R. Wenger. A Randomized O(m log m) Algorithm for Computing Reeb Graphs of Arbitrary Simplicial Complexes. In *ACM Symposium on Computational Geometry*, pages 267–276, 2010.

[25] C. Heine, D. Schneider, H. Carr, and G. Scheuermann. Drawing contour trees in the plane. *IEEE Transactions on Visualization and Computer Graphics*, 17(11):1599–1611, 2011.

[26] W. Hibbard and D. Santek. Visualizing Large Data Sets in the Earth Sciences. *Computer*, 22(8):53–57, 1989.

[27] M. Hilaga, Y. Shinagawa, T. Kohmura, and T. L. Kunii. Topology Matching for Fully Automatic Similarity Estimation of 3D Shapes. *ACM Transactions on Graphics*, pages 203–212, 2001.

[28] S. Maadasamy, H. Doraiswamy, and V. Natarajan. A hybrid parallel algorithm for computing and tracking level set topology. In *High Performance Computing (HiPC), 2012 19th International Conference on*, pages 1–10. IEEE, 2012.

[29] D. Morozov and G. Weber. Distributed merge trees. In *Proceedings of the 18th ACM SIGPLAN symposium on Principles and practice of parallel programming*, PPoPP '13, pages 93–102, New York, NY, USA, 2013. ACM.

[30] S. Nagaraj and V. Natarajan. Simplification of Jacobi Sets. In V. Pascucci, X. Tricoche, H. Hagen, and J. Tierny, editors, *Topological Data Analysis and Visualization: Theory, Algorithms and Applications*, Mathematics and Visualization, pages 91–102. Springer, 2011.

[31] S. Parsa. A Deterministic O(m log m) Time Algorithm for the Reeb Graph. In *ACM Symposium on Computational Geometry*, pages 269–276, 2012.

[32] V. Pascucci and K. Cole-McLaughlin. Parallel Computation of the Topology of Level Sets. *Algorithmica*, 38(2):249–268, 2003.

[33] V. Pascucci, G. Scorzelli, P.-T. Bremer, and A. Mascarenhas. Robust On-line Computation of Reeb Graphs: Simplicity and Speed. *ACM Transactions on Graphics*, 26(3):58.1–58.9, 2007.

[34] G. Reeb. Sur les Points Singuliers d'une Forme de Pfaff Complètement Intégrable ou d'une Fonction Numérique. *Comptes Rendus de l'Acadèmie des Sciences de Paris*, 222:847–849, 1946.

[35] O. Saeki. *Topology of Singular Fibers of Differentiable Maps*. Number 1854 in Lecture Notes in Mathematics. Springer, 2004.

[36] C. E. Scheidegger, J. M. Schreiner, B. Duffy, H. Carr, and C. T. Silva. Revisiting Histograms and Isosurface Statistics. *IEEE Transactions on Visualization and Computer Graphics*, 14(6):1659–1666, 2008.

[37] D. Schneider, A. Wiebel, H. Carr, M. Hlawitschka, and G. Scheuermann. Interactive Comparison of Scalar Fields Based on Largest Contours with Applications to Flow Visualization. *IEEE Transactions on Visualization and Computer Graphics*, 14(6):1475–1482, 2008.

[38] W. Schroeder, K. Martin, and B. Lorensen. *The Visualization Toolkit: An Object-Oriented Approach to 3D Graphics*. Kitware, Inc., fourth edition, 2006.

[39] R. E. Tarjan. Efficiency of a Good but not Linear Set Union Algorithm. *Journal of the ACM*, 22:215–225, 1975.

[40] J. Tierny, A. Gyulassy, E. Simon, and V. Pascucci. Loop Surgery for Volumetric Meshes: Reeb Graphs Reduced to Contour Trees. *IEEE Transactions on Visualization and Computer Graphics*, 15(6):1177–1184, 2010.

[41] M. van Kreveld, R. van Oostrum, C. L. Bajaj, V. Pascucci, and D. R. Schikore. Contour Trees and Small Seed Sets for Isosurface Traversal. In *Proceedings, 13th ACM Symposium on Computational Geometry*, pages 212–220, 1997.

[42] M. J. van Kreveld, R. van Oostrum, C. L. Bajaj, V. Pascucci, and D. R. Schikore. *Topological Data Structures for Surfaces: An Introduction for Geographical Information Science*, chapter 5: Efficient contour tree and minimum seed set construction, pages 71–86. John Wiley & Sons, May 2004.

[43] G. Weber, P.-T. Bremer, and V. Pascucci. Topological Landscapes: A Terrain Metaphor for Scientific Data. *IEEE Transactions on Visualization and Computer Graphics*, 13(6):1416–1423, November/December 2007.

[44] G. Weber, S. Dillard, H. Carr, V. Pascucci, and B. Hamann. Topology-Controlled Volume Rendering. *IEEE Transactions on Visualization and Computer Graphics*, 13(2):330–341, March/April 2007.

[45] G. Weber, G. Scheuermann, and H. Hagen. Detecting Critical Regions in Scalar Fields. In *Proceedings of Eurographics-IEEE Symposium on Visualization 2003*, pages 85–94,288, 2003.

[46] X. Zhang, C. L. Bajaj, and N. Baker. Fast Matching of Volumetric Functions Using Multi-resolution Dual Contour Trees. Technical report, Texas Institute for Computational and Applied Mathematics, Austin, Texas, 2004.

Hamish Carr completed his PhD at the University of British Columbia in May 2004 and has worked as a lecturer at University College Dublin and a senior lecturer at the University of Leeds. His research interests include scientific and medical visualization, computational geometry and topology, computer graphics and geometric applications. He is a member of the IEEE and the IEEE Computer Society and Chair of the UK Chapter of the Eurographics Association.

David Duke David Duke received his PhD from the University of Queensland, Australia in 1992, subsequently working at the Universities of York and Bath in the UK, before joining the visualization group at Leeds in 2004. His research has encompassed formal methods, HCI, and functional programming, but since 2000 his primary interests are visualization systems, graph visualization, and programming technologies. He is a Fellow of the Eurographics Association, and a member of the IEEE and IEEE Computer Society.